Biomaterials 35 (2014) 8927–8936

Contents lists available at ScienceDirect

Biomaterials

journal homepage: www.elsevier.com/locate/biomaterials

Influence of the stiffness of three-dimensional alginate/collagen-I interpenetrating networks on fibroblast biology

Cristiana Branco da Cunha [a, b, c, d, e], Darinka D. Klumpers [a, b, f], Weiwei A. Li [a, b], Sandeep T. Koshy [a, b, g], James C. Weaver [b], Ovijit Chaudhuri [h], Pedro L. Granja [d, i, j], David J. Mooney [a, b, *]

[a] School of Engineering and Applied Sciences, Harvard University, Cambridge, MA 02138, USA
[b] Wyss Institute for Biologically Inspired Engineering, Harvard University, Boston, MA 02115, USA
[c] Institute of Molecular Pathology and Immunology of the University of Porto (IPATIMUP), 4200-465 Porto, Portugal
[d] Instituto de Engenharia Biomédica da Universidade do Porto (INEB), 4150-180 Porto, Portugal
[e] Faculdade de Medicina da Universidade do Porto (FMUP)/Hospital S. João, 4200-319 Porto, Portugal
[f] Dept. Orthopedic Surgery, Research Institute MOVE, VU University Medical Center, 1081 HV, Amsterdam, The Netherlands
[g] Harvard-MIT Division of Health Sciences and Technology, Cambridge, MA 10239, USA
[h] Department of Mechanical Engineering, Stanford University, Stanford, CA 94305, USA
[i] Departamento de Engenharia Metalúrgica e Materiais, Faculdade de Engenharia da Universidade do Porto (FEUP), 4200-465 Porto, Portugal
[j] Instituto de Ciências Biomédicas Abel Salazar da Universidade do Porto (ICBAS), 4050-313 Porto, Portugal

ARTICLE INFO

Article history:
Received 15 May 2014
Accepted 25 June 2014
Available online 19 July 2014

Keywords:
Wound healing
ECM (extracellular matrix)
Mechanical properties
Interpenetrating networks (IPNs)
Inflammation
Wound dressing biomaterial

ABSTRACT

Wound dressing biomaterials are increasingly being designed to incorporate bioactive molecules to promote healing, but the impact of matrix mechanical properties on the biology of resident cells orchestrating skin repair and regeneration remains to be fully understood. This study investigated whether tuning the stiffness of a model wound dressing biomaterial could control the behavior of dermal fibroblasts. Fully interpenetrating networks (IPNs) of collagen-I and alginate were fabricated to enable gel stiffness to be tuned independently of gel architecture, polymer concentration or adhesion ligand density. Three-dimensional cultures of dermal fibroblasts encapsulated within matrices of different stiffness were shown to promote dramatically different cell morphologies, and enhanced stiffness resulted in upregulation of key-mediators of inflammation such as IL-10 and COX-2. These findings suggest that simply modulating the matrix mechanical properties of a given wound dressing biomaterial deposited at the wound site could regulate the progression of wound healing.

1. Introduction

Wound healing is a complex physiological process orchestrated by multiple cell types, soluble factors and extracellular matrix (ECM) components [1]. Most cutaneous injuries heal rapidly within a week or two, though often leading to the formation of fibrotic scar tissue which is neither aesthetically desirable nor functional [2]. However, several pathogenic abnormalities, ranging from diabetic ulcers to infection or continued trauma, contribute to failure to heal [3]. Chronic non-healing wounds are a cause of significant morbidity and mortality, and constitute a huge burden in public health care with estimated costs of more than $3 billion per year in the United States [4]. The goal of wound care therapies is to regenerate tissues such that the structural and functional properties are restored to the levels prior to injury [5]. The use of biomaterials as scaffolds for skin healing is a successful long-lasting concept [6], as demonstrated by the use of porous crosslinked networks of collagen and glycosaminoglycans (GAG) which induced full regeneration of functional skin within 4 weeks [7,8]. Currently, wound dressing biomaterials often incorporate antimicrobial, antibacterial, and anti-inflammatory agents [9] to further aid and enhance natural skin healing. The wound dressing market is expanding rapidly as it becomes clear that no single dressing is suitable for all wounds, and that their physiochemical properties can be manipulated to target the different stages of the healing process [10].

Following a skin injury, disruption of the tissue architecture leads to a dramatically altered mechanical context at the site of the wound [11]. Mechanical cues in the wound microenvironment can

* Corresponding author. School of Engineering and Applied Sciences, Harvard University, 29 Oxford St., 319 Pierce Hall, Cambridge, MA 02138, USA. Fax: +1 617 495 9837.
E-mail address: mooneyd@seas.harvard.edu (D.J. Mooney).

http://dx.doi.org/10.1016/j.biomaterials.2014.06.047
0142-9612/

guide the behavior of a milieu of infiltrating cells such as recruited immune cells [12] and fibroblasts [14]. Mechanical cues are also known to sponsor or hinder different stages of the wound repair response, from epithelial morphogenesis [15] to blood vessel formation [16]. However, the importance of mechanical forces in the context of wound dressing design has been often overlooked.

In this study we investigated if one could control the behavior of dermal fibroblasts involved in the wound healing response by simply tuning the storage modulus of a model wound dressing biomaterial. Numerous material systems have been developed to help understand how ECM mechanics regulate cell behaviors, from migration [17,18] to differentiation [19,20]. However, these material systems do not always allow one to perform three-dimensional cell cultures where matrix stiffness is decoupled from scaffold architecture, polymer concentration or adhesion ligand density. One way to achieve this separation is through the design of interpenetrating network (IPN) hydrogels, which consist of two or more polymer networks that are not covalently bonded but at least partially interlaced [21]. We developed a biomaterial system composed of IPNs of collagen-I and alginate; both of these components are widely used in the tissue engineering field. The sodium alginate polymeric backbone presents no intrinsic cell-binding domains, but can be used to regulate gel mechanical properties. The collagen-I presents specific peptide sequences recognized by cell surface receptors, and provides a substrate for cell adhesion that better recreates many *in vivo* contexts. Encapsulated cells sense, adhere and pull on the collagen-I fibrils and depending on the degree of crosslinking of the intercalated alginate mesh, it is expected they will feel more or less resistance to deformation from the matrix. The alginate backbone is ionically crosslinked by divalent cations (in this case, Ca^{2+}), thus solely changing the concentration of calcium modulates the stiffness of the IPN. *In vivo*, fibroblasts are recruited to the wound site for the synthesis, deposition and remodeling of the new ECM [1], being one of the most important cell mediators of the wound healing response. Hence in this study we assessed the *in vitro* behavior of primary dermal fibroblasts isolated from the dermis of healthy non-diabetic donors when encapsulated within IPNs of varying stiffness, to partially mimic the effects of mechanical cues on the response of fibroblasts migrating into a wound site *in vivo*.

2. Materials and methods

2.1. Cell culture

Human dermal fibroblasts (ZenBio) were cultured according to the manufacturer's protocol, and used between passages 6 and 11. For routine cell culture, cells were cultured in dermal fibroblasts culture medium (ZenBio), a DMEM-based culture medium containing fetal bovine serum, 4.15 g/L D-glucose, penicillin, streptomycin and amphotericin B. The manufacturer also reports the addition of specific growth factors necessary for optimal expansion of human dermal fibroblasts. Cells were maintained at sub-confluence in the incubator at 37 °C and 5% CO_2. The culture medium was refreshed every three days.

2.2. Alginate preparation

High molecular weight (LF20/40) sodium alginate was purchased from FMC Biopolymer. Alginate was dialyzed against deionized water for 2–3 days (molecular weight cutoff of 3500 Da), treated with activated charcoal to remove any contaminants, sterile filtered (0.22 μm), lyophilized, and then reconstituted in serum-free DMEM medium at 2.5% w/v. RGD-decorated alginate was prepared using carbodiimide chemistry to couple the oligopeptide GGGGRGDSP (Peptides International) to the alginate, such that on average 20 RGD peptides were coupled to each alginate polymer [22].

2.3. IPNs preparation

All IPNs in this study consisted of 1.5 mg/ml rat-tail collagen-I (BD Biosciences), and 5 mg/ml high molecular weight alginate. The IPN matrix formation process consisted of two steps. In the first step, reconstituted alginate (2.5% w/v in serum-free DMEM medium) was delivered into a centrifuge tube and put on ice. Rat-tail collagen-I was mixed with a 10× DMEM solution in a 1:10 ratio to the amount of collagen-I needed and the pH was adjusted to 7.4 using a 1 M NaOH solution. The final concentration of rat-tail collagen-I in the IPN was adjusted to 1.5 mg/ml using serum-free DMEM. The rat-tail collagen-I solution was then thoroughly mixed with the alginate solution. Once the collagen-alginate mixture was prepared, the human dermal fibroblasts were washed, trypsinized (0.05% trypsin/EDTA, Invitrogen), counted using a Z2 Coulter Counter (Beckman Coulter), resuspended at a concentration of 3×10^6 cells per ml in cell culture medium and mixed with the collagen-alginate mixture. The collagen-alginate-cells mixture was then transferred into a pre-cooled 1 ml luer lock syringe (Cole-Parmer).

In the second step, a solution containing calcium sulfate dihydrate ($CaSO_4.2H_2O$, Sigma), used to crosslink the alginate network, was prepared as follows. Calcium sulfate dihydrate was reconstituted in water at 1.22 M and autoclaved. For each IPN, 100 μl of DMEM containing the appropriate amount of the calcium sulfate slurry was added to a 1 ml luer lock syringe. The syringe with the calcium sulfate solution was agitated to mix the calcium sulfate uniformly, and then the two syringes were connected together with a female–female luer lock coupler (Value Plastics). The two solutions were mixed and immediately deposited into a well of a 48-well plate. The plate was then transferred to the incubator at 37 °C and 5% CO_2 for 60 min to allow gelation, after which culture medium was added to each gel. Culture medium was refreshed every two days for the duration of each experiment.

2.4. Scanning electron microscopy

For scanning electron microscopy (SEM), IPNs were fixed in 4% paraformaldehyde (PFA), washed several times in PBS, and serially transitioned from dH_2O into absolute ethanol with 30 min incubations in 30, 50, 70, 90, and 100% ethanol solutions. Ethanol dehydrated IPNs were dried in a critical point dryer and adhered onto sample stubs using carbon tape. Samples were sputter coated with 5 nm of platinum–palladium and imaged using secondary electron detection on a Carl Zeiss Supra 55 VP field emission scanning electron microscope.

2.5. Elemental analysis

For elemental analysis, IPNs were fixed in 4% paraformaldehyde (PFA), washed several times in PBS, quickly washed with dH_2O, froze overnight at −20 °C and lyophilized. Elemental analysis, via Energy Dispersive Spectroscopy (EDS), was performed using a Tescan Vega3 scanning electron microscope equipped with a Bruker Nano XFlash 5030 silicon drift detector.

2.6. Mechanical characterization of IPNs

The mechanical properties of the IPNs were characterized with an AR-G2 stress controlled rheometer (TA Instruments). IPNs and collagen-I hydrogels without cells were formed as described above, and directly deposited onto the pre-cooled surface plate of the rheometer. A 20 mm plate was immediately brought into contact before the IPN started to gel, forming a 20 mm disk of IPN. The plate was warmed to 37 °C, and the mechanical properties were then measured over time as described previously [23]. Briefly, the storage modulus at 0.5% strain and at 1 Hz was recorded periodically until it reached its equilibrium value (30–40 min, Fig. S2). A strain sweep was performed to confirm that this value was within the linear elastic regime, followed by a frequency sweep. Further quantitative analysis on the viscoelastic properties of these IPNs was performed as follows. Phase angle δ, defined as $\delta = \tan^{-1}(G''/G')$, was calculated based on the measured G' and G'' at 0.1 Hz. The frequency dependent rheology of the gels followed a weak power law of the form $G' \sim f^{\alpha}$. The power law exponent α was calculated by fitting the frequency dependence of G' of each measurement to this equation. This power law relationship is characteristic of many biological materials, including cells and reconstituted actin networks [24,25], and provides a useful parameter with which to characterize the viscoelasticity of the gels.

2.7. Analysis of macromolecular transport in IPNs

The diffusion coefficient of 70 kDa fluorescently labeled anionic dextran (Invitrogen) through IPNs used in this study was determined. For these studies, IPNs of varying mechanical properties encapsulating 0.2 mg/ml fluorescein-labeled dextran were prepared in a standard tissue culture 48-well plate. IPNs were allowed to equilibrate at 37 °C for 1 h, before serum-free phenol red-free DMEM medium was added to the well. Aliquots of this media were taken periodically to measure the molecular diffusion of dextran from the hydrogels into the media. Samples were continuously agitated using an orbital shaker, and fluorescein-labeled dextran concentration was measured using a fluorescence plate reader (Biotek). The measurements were interpreted using the semi-infinite slab approximation as described previously [26].

2.8. Immunohistochemistry

The IPNs were fixed in 4% paraformaldehyde for 1 h at room temperature and washed in PBS overnight at 4 °C. The IPNs were embedded in 2.5% low gelling temperature agarose (Lonza) by placing the gels in liquid agarose in a 40 °C water bath for several hours and subsequent gelling at 4 °C. A Leica vibratome was used to cut 200 μm sections. To visualize the general protein content and distribution

within the IPN gels, Fast Green staining was performed. Vibratome sections were rinsed in dH_2O, stained for 2 min with 0.2% Fast Green FCF (aqueous, Electron Microscopy Sciences), rapidly rinsed in 1% acetic acid and subsequently washed in dH_2O. To visualize the distribution of alginate within the IPN gels, gels were made using FITC-labeled alginate. To visualize the distribution of collagen-I fibers within the IPN gels, the collagen meshwork was probed with a rabbit anti-collagen-I polyclonal antibody (Abcam) and stained with an AlexaFluor© 647 conjugated goat-anti-rabbit IgG, after vibratome sectioning. The F-actin cytoskeleton of embedded cells was visualized by probing cross-sections with AlexaFluor© 488 conjugated phalloidin (Invitrogen). Cell nuclei were stained with Hoechst 33342 (Invitrogen). Fluorescent micrographs were acquired using an Upright Zeiss LSM 710 confocal microscope.

2.9. Cell retrieval for gene expression and flow cytometry analyses

To retrieve the fibroblasts encapsulated within the IPN, the culture media was first removed from the well and the IPNs were washed once with PBS. Next, the IPNs were transferred into a falcon tube containing 10 ml of 50 mM EDTA in PBS in which they remained for 30 min on ice. The resulting solution was then centrifuged and the supernatant removed. The remaining gel pieces were then incubated with a solution of 500 U/mL Collagenase type IV (Worthington) in serum-free DMEM medium for 30 min at 37 °C and 5% CO_2 and vigorously shaken to help disassociate the gels. The resulting solution was then centrifuged and the enzyme solution removed. The cell pellet was immediately placed on ice.

For RNA expression analysis, the retrieved cells were then lysed using Trizol, and RNA was extracted following the manufacturer's guidelines (Life Technologies). For flow cytometry, the cell pellet was resuspended and filtered though a 40 μm cell strainer and then analyzed a using a BD LSR II flow cytometer instrument. A monoclonal anti-human integrin β1 (CD29) PE-conjugated (clone TS2/16, BioLegend) was used. An anti-mouse IgG1, κ (clone MOPC-21, BioLegend) was used as an isotype control. A monoclonal anti-human COX-2 antibody (clone AS66, Abcam) was used, followed by an AlexaFluor© 647 conjugated goat-anti-mouse IgG secondary antibody (Life Technologies).

2.10. qPCR

RNA was quantified using a NanoDrop ND-1000 Spectrophotometer. Reverse transcription was carried out with the RT2 First Strand Kit (Qiagen); 500 ng of total RNA were used per sample. The expression profile of a panel of genes was assessed with the Human Wound Healing PCR Array (Qiagen), on a 96-well plate format and using an ABI7900HT thermocycler (Applied Biosystems).

2.11. ELISA

Cell supernatant was collected and analyzed for IL-10 using ELISA (eBioscience 88-7106) according to manufacturer's directions. Briefly, high binding 96-well plates (Costar 2592) were coated with anti-human IL-10 and subsequently blocked with bovine serum albumin (BSA). IL-10 standards and supernatant were loaded and detected with biotin-conjugated anti-human IL-10. At least 4 replicates were used for each condition.

3. Results

3.1. Interpenetrating networks (IPNs) characterization

IPNs of alginate and collagen-I were fabricated to tune ECM stiffness independently of ECM composition or structure, and primary dermal fibroblasts were encapsulated therein (Fig. 1).

The microarchitecture of the alginate/collagen-I IPNs was assessed by SEM. Hydrogels composed entirely of 5 mg/ml of alginate showed an interconnected nanoporous scaffold structure (Fig. 2A), while hydrogels composed entirely of 1.5 mg/ml collagen-I revealed a highly porous, randomly organized fibrillar network (Fig. 2A). The alginate/collagen-I IPNs confirmed the interpenetration of both components, with a nanoporous alginate mesh fully intercalated by multidirectional collagen-I fibrils (Fig. 2A). The dehydration and drying steps used to prepare the samples for SEM can cause shrinkage and, consequently, collapse of the porous structure of the hydrogels; however, since all samples were processed simultaneously and in the same fashion, these effects are expected to be similar across all the different conditions analyzed.

The alginate network was crosslinked by divalent cations of calcium (Ca^{2+}) that preferentially intercalate between the guluronic acid residues ("G-blocks"). Elemental mapping analysis of alginate/collagen-I IPNs, crosslinked to different extents with calcium sulfate solution, confirmed that different amounts of calcium were present inside the IPN (Fig. 2B). The amount of calcium detected in the sample for which no calcium sulfate was added is likely due to residual amounts of calcium ions present in the culture media in which the hydrogels were immersed to equilibrate overnight.

To establish the micro-scale distribution of the alginate chains within the IPNs, FITC-labeled alginate mixed with unlabeled collagen-I was visualized by confocal microscopy. In order to prevent any disruption of the alginate mesh architecture the hydrogels were not washed, fixed or sectioned, but rather imaged directly after 1 h of gelation at 37 °C. The mixture of the two

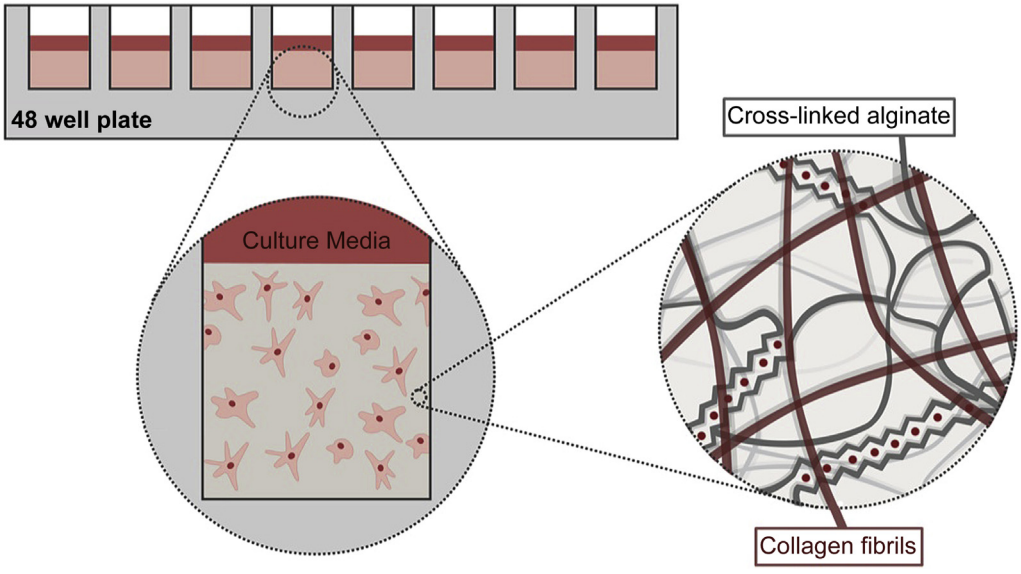

Fig. 1. Schematic of primary dermal fibroblasts encapsulated within IPNs of alginate and collagen-I (red fibers). Inset illustrates a schematic of the calcium ions (red dots) crosslinking the G-blocks of the alginate network (black zig-zag structures). As zonal ionic crosslinking increases, the IPN architecture and pore size remains unchanged. Objects in figure are not drawn to scale (For interpretation of the references to color in this figure legend, the reader is referred to the web version of this article.).

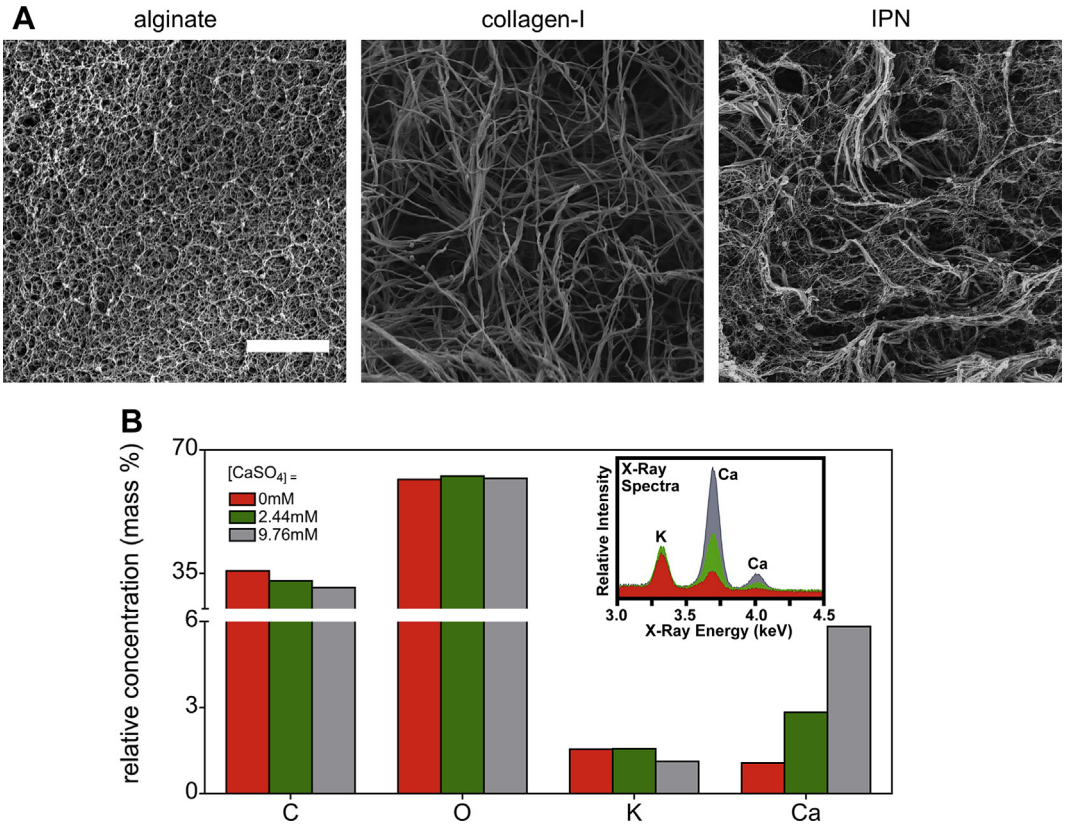

Fig. 2. Analysis of microarchitecture of IPNs of alginate and collagen-I reveals full intercalation of both polymer networks. (A) Scanning electron micrograph of a hydrogel composed of alginate only, a hydrogel composed of collagen-I only and an IPN of alginate and collagen-I at the same polymer concentrations as hydrogels containing only one of the polymers. Scale bar is 2 μm. (B) Using C, O, and K as internal standards, energy dispersive spectroscopy was used to qualitatively detect different degrees of Ca^{2+} incorporation within alginate/collagen-I IPNs at three different levels of calcium crosslinking. A composite EDS spectrum is included as an inset.

components showed no micro-scale phase separation for all levels of calcium crosslinking studied (Fig. 3A, Fig. S1A), as shown in the histogram of fluorescent alginate intensity per pixel. Furthermore, Fast Green staining was used to allow visualization of the protein content within the IPNs. Protein staining was uniform throughout the entire cross-section of these hydrogels, across the range of calcium crosslinking used (Fig. 3B, Fig. S1B), as shown in the histogram of Fast Green intensity per pixel. A slight change in the peak location on the Fast Green intensity histogram was observed between the soft (crosslinked with 2.44 mM $CaSO_4$) and the stiff (crosslinked with 9.76 mM $CaSO_4$) samples, but the presence of only one peak in both samples indicates that there is no phase separation in the protein content along the hydrogel. Finally, staining with anti-collagen-I antibody was used to visualize the microarchitecture of the collagen network. Confocal fluorescence microscopy revealed, as expected, a homogenous fibrillar mesh of collagen-I throughout the entire cross-section of these hydrogels, without any distinct patches of collagen-I (Fig. 3C). These results together indicate that the networks were indeed fully interpenetrating, independently of the degree of crosslinking of the alginate component.

To determine whether tuning the alginate crosslinking by varying the calcium concentration caused changes in gel pore size, macromolecular transport through the IPNs was analyzed. Specifically, the diffusion coefficient of anionic high molecular weight dextran (70 kDa) through the various hydrogels was measured. No statistically significant differences in the diffusion coefficient of the dextran among the various IPNs of different stiffness were found (Fig. 3D), indicating that the pore size remained constant as the concentration of calcium was varied.

3.2. Mechanical properties of IPNs

The mechanical properties of the alginate/collagen-I IPNs were assessed by rheology to confirm that variations in calcium crosslinking would yield hydrogels with different moduli. At a fixed frequency of 1 Hz across a time period of 60 min, the storage modulus could be tuned from 50 to 1200 Pa by merely changing the initial concentration of calcium, while maintaining a constant polymer composition (Fig. 4A). The storage modulus of the pure collagen-I hydrogels and the alginate/collagen-I IPN with none or low amounts (2.44 mM) of $CaSO_4$ showed no statistically significant differences (One-Way ANOVA with Dunnett's post-hoc test, $p > 0.05$), and were considered to be equivalent. The frequency dependent storage moduli of the different IPNs indicated that all IPNs exhibited some degree of viscoelasticity (Fig. 4B). However, the storage modulus is much greater than the loss modulus, and the storage modulus exhibits only a very weak dependence on the frequency, indicating that the overall mechanical response for these IPNs is predominantly elastic over a frequency range of 0.1 Hz–1 Hz (Fig. S2A). The time course of IPNs gelation across a range of calcium crosslinker concentrations was further assessed, and complete gelation of the matrices was achieved after 30–40 min at 37 °C (Fig. S2B).

3.3. Effects of stiffness on fibroblasts morphology

Human adult dermal fibroblasts isolated from the dermis of healthy non-diabetic donors were subsequently encapsulated within these alginate/collagen-I IPNs to examine the impact of gel mechanical properties on cell biology. Fibroblasts showed an

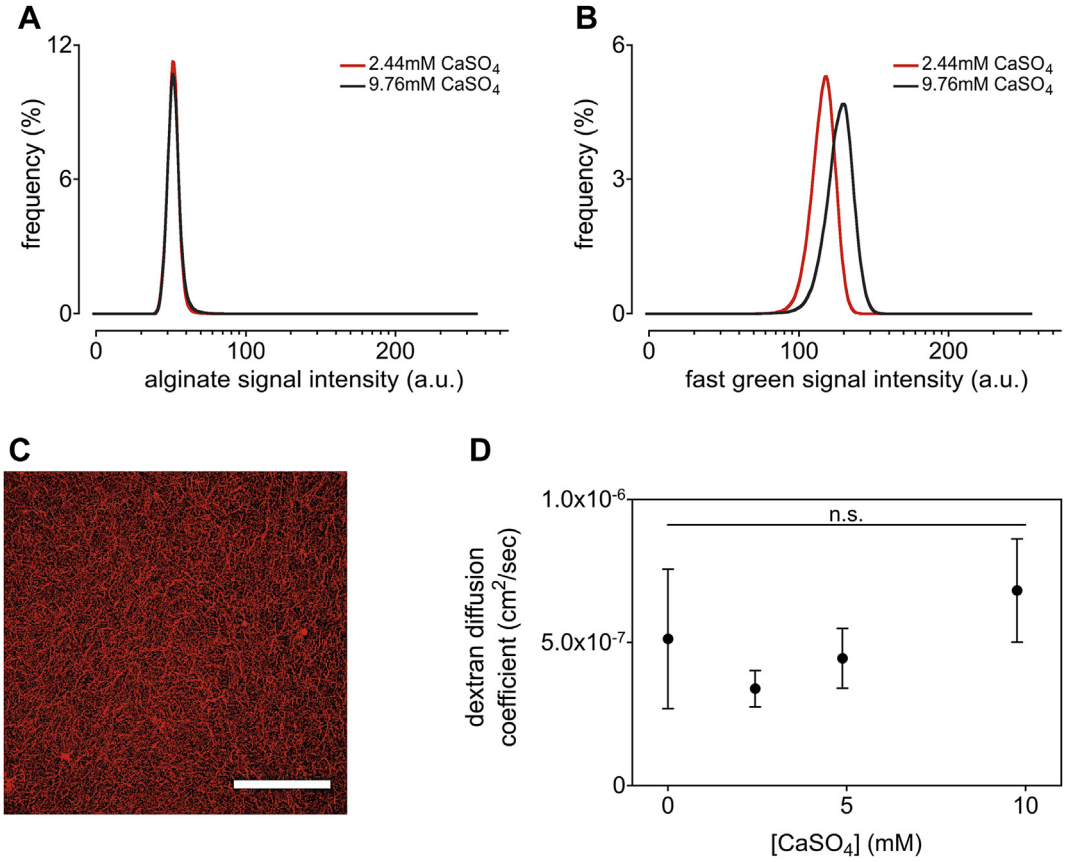

Fig. 3. IPNs of alginate and collagen-I demonstrate no micro-scale phase separation nor differences in gel porosity as calcium crosslinking is varied. (A) Histogram of fluorescently labeled alginate intensity per pixel taken from 2 independent images of hydrogels at two different levels of calcium crosslinking. (B) Histogram of Fast Green staining intensity per pixel taken from 4 independent images of hydrogels at two different levels of calcium crosslinking. The presence of a single peak in both histograms demonstrates that there is no micro-scale phase separation in the IPNs. (C) Representative micrograph of confocal immunofluorescence imaging of collagen-I antibody staining of a cross-section of alginate/collagen-I IPN. Scale bar is 100 μm. (D) Diffusion coefficient of fluorescently labeled 70 kDa dextran as a function of calcium crosslinking in IPNs. Differences are not statistically significant (n.s.) (One-Way ANOVA with Tukey's post-hoc test, $p > 0.05$). Data are shown as mean and standard deviation of three independent experiments.

elongated, spindle-like morphology after a few hours of culture within the gels of lowest storage modulus (Fig. 5A). These softer matrices contracted after a few days of culture, suggesting that the encapsulated cells are potentially able to pull on the matrix and contract it (Fig. S3A). In IPNs of increased stiffness fibroblasts exhibited a spherical shape (Fig. 5A), up to at least 5 days of culture. Fibroblasts encapsulated within IPNs of intermediate stiffness (320 Pa) also remained spherical after 48 h of culture, suggesting a bimodal effect of the stiffness of this particular biomaterial system on fibroblasts morphology (Fig. S3B). These effects were not due to the higher concentrations of calcium in the stiffer IPNs, as when the highest amount of calcium sulfate (9.76 mM) was incorporated within hydrogels containing only collagen-I and dermal fibroblasts, cells were still able to spread and contract the matrix (Fig. S3C).

The fibroblasts encapsulated inside IPNs of different moduli were then retrieved and analyzed after 48 h of culture. No statistically significant differences regarding cell number between matrices of different storage modulus were observed (Fig. S4A), and

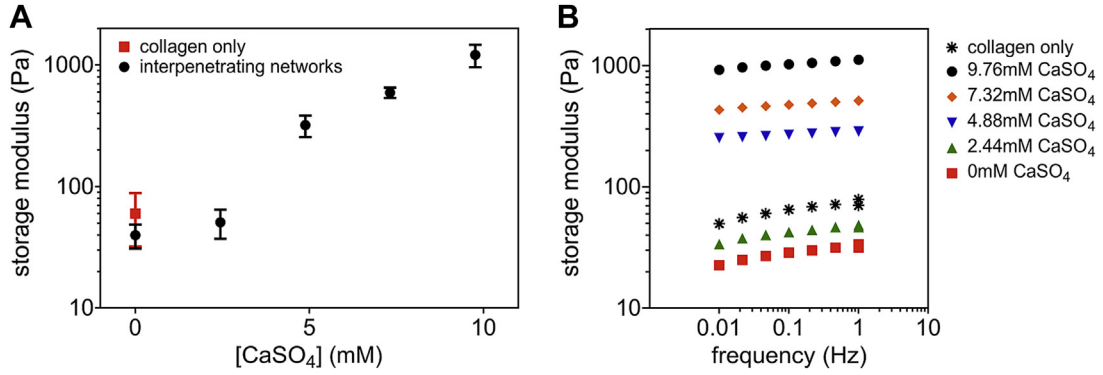

Fig. 4. Storage modulus of IPNs of alginate and collagen-I can be modulated by the extent of calcium crosslinking. (A) Storage modulus at 1 Hz as a function of calcium crosslinking in IPNs. Data are shown as mean and standard deviation ($n = 3–5$). (B) Frequency dependent rheology of IPNs at the indicated concentrations of calcium crosslinker, after gelation was completed. Data is representative of at least three measurements for each condition.

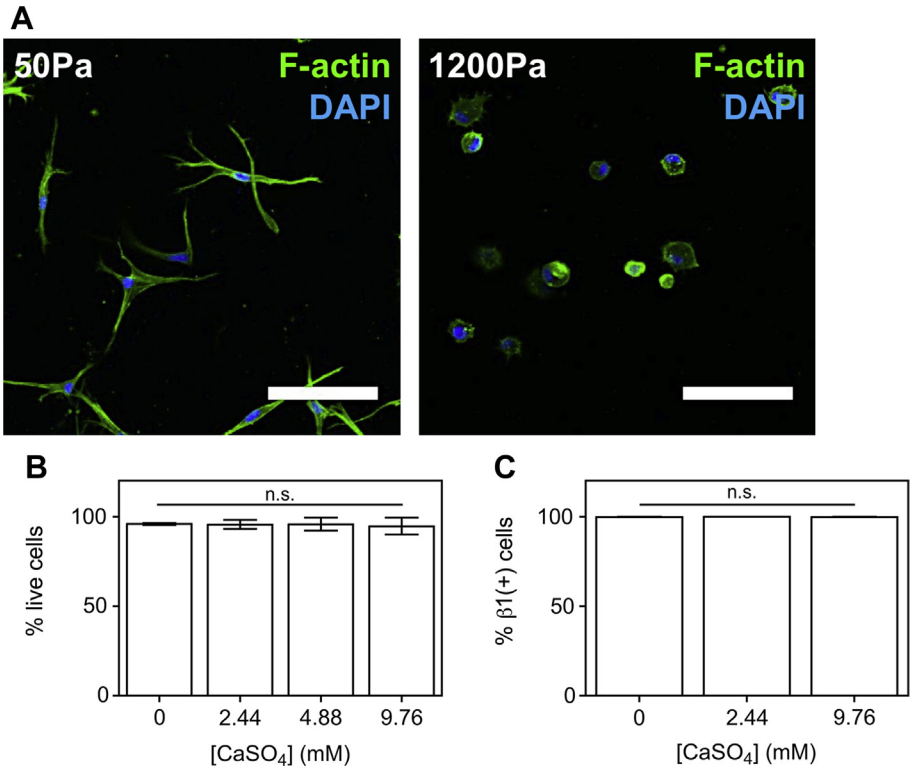

Fig. 5. Different storage moduli lead to dramatic changes in cell morphology, without affecting cell viability or collagen-I integrin receptor expression. (A) Representative micrographs of confocal immunofluorescence imaging of the cell cytoskeleton, as shown by fluorescent F-actin staining, in cross-sections of alginate/collagen-I IPNs with storage modulus of 50 and 1200 Pa. DAPI staining is shown in blue. Scale bars are 100 μm. (B) Flow cytometry analysis of viability of cells recovered from IPNs crosslinked at varying calcium concentrations ($n = 7–10$). (C) Flow cytometry analysis of β1-integrin antibody staining of cells recovered from IPNs crosslinked with varying concentrations of calcium ($n = 3$). Differences are not statistically significant (n.s.) (One-Way ANOVA with Tukey's post-hoc test, $p > 0.05$). Data are shown as mean and standard deviation in all plots. All data was collected after cells were encapsulated for 48 h.

over 95% of the cells encapsulated in IPNs of different moduli were alive after 48 h of culture (Fig. 5B). As the attachment of primary fibroblasts to collagen type I is mediated by non-RGD-dependent β1 integrin matrix receptors [27], flow cytometry measurements were used to analyze expression of this cell surface receptor. All the cells encapsulated in IPNs of different moduli expressed integrin β1 receptors, with no significant differences between their mean fluorescence intensity (Fig. 5C, Fig. S4B).

To examine potential effects of altered cell adhesion ligand density in IPNs on fibroblast morphology, RGD cell adhesion motifs were coupled to the alginate prior to IPN formation. No differences in the morphology of encapsulated fibroblasts between IPNs composed of unmodified and RGD-modified alginate chains were observed, independently of the moduli tested (Fig. S4C).

3.4. Effect of stiffness on wound healing genetic programs

We next sought to elucidate if the dramatic changes in cell spreading are accompanied by different gene expression profiles. Real-time reverse transcription polymerase chain reaction (RT-PCR) was used to analyze the expression of a panel of 84 genes that are known to ECM remodeling factors, inflammatory cytokines and chemokines, as well as key growth factors and major signaling molecules (Table 1). The gene screening revealed 12 genes displaying a statistically significant 2-fold difference in gene expression between dermal fibroblasts encapsulated in IPNs of 1200 *versus* 50 Pa (Fig. 6A). The expression of 2 genes was downregulated, and the expression of 10 genes was upregulated. The genes that were downregulated were chemokine ligand 2 (*CCL2*) and transgelin (*TAGLN*). Three other genes, colony stimulating factor 2 (*CSF2*), connective tissue growth factor (*CNTG*) and matrix metallopeptidase 9 (*MMP-9*) were dowregulated, but the fold-change difference was not statistically significant. A subset of the upregulated genes is known to be involved in inflammation cascades: interleukin 10 (*IL10*), interleukin 1β (*ILB1*), and prostaglandin-endoperoxide synthase 2 (*PTGS2*) also known as *COX2*. A subset of collagen encoding genes was also upregulated: collagen type IV, alpha 1 (*COL4A1*) and collagen type V, alpha 3 (*COL5A3*). Another subset of upregulated genes represents cell adhesion and ECM molecules: integrin α4 (*ITGA4*), matrix metallopeptidase 1 (*MMP1*) and vitronectin (*VTN*). The remaining upregulated genes were hepatocyte growth factor (*HGF*) and a member of the WNT gene family (*WNT5A*). Expression of collagen type IV, alpha 3 (*COL4A3*) was increased, but the effects were not statistically significant.

To validate the gene expression results, protein expression for IL-10 and COX-2 were analyzed. The amount of IL-10 protein secreted into the culture medium by dermal fibroblasts encapsulated in IPNs of different storage moduli was measured by ELISA (Fig. 6B), and enhanced matrix stiffness promoted a 3-fold increase in the production and secretion of this anti-inflammatory cytokine. Stiffening of the matrix also led to an increase in the number of cells expressing COX-2 (Fig. 6C), and an increase in the expression level in the cells staining positive for this inflammation-associated enzyme (Fig. S5A).

4. Discussion

IPNs of alginate and collagen-I were developed to decouple the effects of gel stiffness on resident fibroblasts from the impact of gel architecture, porosity and adhesion ligand density. Extensive characterization of the microarchitecture of the alginate/collagen-I

Table 1
mRNA expression analyses of 84 genes involved in the wound healing response by cells encapsulated in IPNs with storage modulus of 50 or 1200 Pa. Data is shown as fold-change in stiff *versus* soft matrices ($n = 3$). In bold are shown the 12 genes displaying a statistically significant 2-fold difference in gene expression (Student's t test, $p < 0.05$).

	Gene symbol	Fold change	p value		Gene symbol	Fold change	p value
1	ACTA2	−1.1699	0.08442	43	IL4	−1.07704	0.97514
2	ACTC1	−1.218	0.38067	44	IL6	1.11133	0.62067
3	ANGPT1	1.03464	0.6922	45	IL6ST	−1.0335	0.61817
4	**CCL2**	**−2.03587**	**0.03785**	46	ITGA1	1.13426	0.24108
5	CCL7	1.52689	0.0855	47	ITGA2	−1.00879	0.90698
6	CD40LG	1.31725	0.04154	48	ITGA3	1.89563	0.13309
7	CDH1	−1.01781	0.89168	49	**ITGA4**	**2.37693**	**0.0059**
8	COL14A1	1.11638	0.57112	50	ITGA5	1.80899	0.00247
9	COL1A1	−1.17728	0.39457	51	ITGA6	−1.36994	0.17954
10	COL1A2	1.00688	0.89218	52	ITGAV	1.15164	0.28612
11	COL3A1	−1.07878	0.42574	53	ITGB1	1.29248	0.06751
12	**COL4A1**	**2.14616**	**0.01752**	54	ITGB3	1.83981	0.0038
13	COL4A3	2.25414	0.07202	55	ITGB5	1.20446	0.04965
14	COL5A1	1.02294	0.95871	56	ITGB6	1.33401	0.17827
15	COL5A2	1.17629	0.02916	57	MAPK1	1.35899	0.03214
16	**COL5A3**	**2.41564**	**0.00479**	58	MAPK3	1.43241	0.07246
17	CSF2	−6.53084	0.09862	59	MIF	1.14898	0.29518
18	CSF3	1.88249	0.2237	60	**MMP1**	**2.03826**	**0.00329**
19	CTGF	−5.92403	0.0721	61	MMP2	1.33303	0.0721
20	CTNNB1	1.56895	0.09087	62	MMP7	1.70224	0.03198
21	CTSG	1.16111	0.38321	63	MMP9	−2.07641	0.33877
22	CTSK	1.21639	0.11425	64	PDGFA	−1.06276	0.66223
23	CTSL2	−1.92854	0.05076	65	PLAT	1.02198	0.99719
24	CXCL1	−1.3196	0.11103	66	PLAU	−1.34385	0.18089
25	CXCL11	−1.35744	0.49611	67	PLAUR	1.0973	0.29239
26	CXCL2	−1.15786	0.4487	68	PLG	−1.01662	0.82105
27	CXCL5	1.0894	0.88231	69	PTEN	1.0636	0.56453
28	EGF	1.38324	0.46425	70	**PTGS2**	**7.5457**	**0.00012**
29	EGFR	1.04159	0.80772	71	RAC1	−1.12853	0.01366
30	F13A1	−1.00967	0.90169	72	RHOA	−1.09249	0.36806
31	F3	−1.61121	0.15939	73	SERPINE1	1.12435	0.35024
32	FGA	1.16111	0.38321	74	STAT3	1.59261	0.00398
33	FGF10	1.39948	0.4891	75	**TAGLN**	**−2.84466**	**0.01566**
34	FGF2	1.39881	0.19275	76	TGFA	1.70906	0.15601
35	FGF7	1.22485	0.00958	77	TGFB1	1.78512	0.00748
36	HBEGF	−1.03724	0.88025	78	TGFBR3	−1.09604	0.3497
37	**HGF**	**4.36136**	**0.0014**	79	TIMP1	−1.01392	0.8633
38	IFNG	1.16111	0.38321	80	TNF	1.61418	0.50605
39	IGF1	−1.26645	0.46731	81	VEGFA	1.87623	0.00203
40	**IL10**	**3.48862**	**0.01998**	82	**VTN**	**2.48098**	**0.00933**
41	**IL1B**	**2.83728**	**0.01768**	83	WISP1	1.45448	0.08059
42	IL2	1.16111	0.38321	84	**WNT5A**	**2.12248**	**0.01082**

IPNs revealed that the degree of calcium crosslinking did not change gel architecture or porosity, as expected since the polymer concentration in the system remains constant. These IPNs present a constant number of adhesion ligand sites, since the concentration of collagen-I remains constant and the alginate backbone presents no binding motifs to which cells can adhere. Macromolecular transport studies demonstrated that diffusion of small metabolites is not affected by the extent of calcium crosslinking of the alginate component, consistently with previous transport studies on alginate gels [20]. Previous studies have focused on the development of biologically inert polymer hydrogels composed of alginate [20], hyaluronic acid [28], and polyethylene glycol [29,30], which allow one to present synthetic adhesion ligands while independently tuning matrix stiffness. However, more complex ECM adhesion elements may be required to closely mimic the biological tissue microenvironment. To address this possibility, material systems that combine entire cell adhesive matrix molecules with synthetic polymers have been emerging in the field of biomaterials [31]. Similar to the approach here described here, IPNs of two different polymers where one is responsible for controlling mechanical properties, and other presents ECM signaling elements, have been previously described [32–36]. In these material systems, however, increasing or decreasing the polymer concentration tunes the scaffold bulk stiffness, but also changes its architecture and porosity. For example, the mechanical properties of collagen-I-containing IPNs have been tuned by adding various quantities of agarose [37]. An approach similar to the one described here was recently reported, in which a gelatin network was crosslinked by transglutaminase and an intercalated alginate network was crosslinked by calcium ions [38]; however, the impact of solely changing the extent of calcium crosslinking in that system was not investigated. In the alginate/collagen-I IPN system presented here, the storage modulus could be tuned from 50 to 1200 Pa by solely controlling the extent of crosslinking with calcium. Furthermore these IPNs showed viscoelastic behavior, as observed in skin [39]. The storage modulus measured by rheology for pure collagen-I hydrogels used in these studies was within the range of moduli described in the literature [40]. Slight variations from the literature may result from the dependence of gel mechanical properties on a number of different parameters ranging from animal age [41], gel thickness [42], or pH [43] and temperature [40] during gelation; these may vary between studies and are difficult to measure precisely within the geometry of the rheometer. It should be noted that this study was limited to the first 48 h of cell culture as these IPNs are prone to cellular-mediated matrix cleavage and remodeling, resulting in changes in the physical properties of the IPNs over time.

Adult dermal fibroblasts showed dramatic differences in cell morphology once immobilized in alginate/collagen-I IPNs of various moduli. The cells spread extensively in soft substrates, but remained round in IPNs of higher stiffness. Cells probe the mechanical properties of their adhesion substrate, and also dynamically reorganize their cytoskeleton in response to the resistance that they detect [44]. Fibroblasts are well known to sense and respond to the compliance of their substrate [45]. At a low degree of calcium crosslinking (50 Pa) the resistance of the matrix to deformation is presumably low enough to allow cells to spread and contract the surrounding gel. Fibroblasts cultured in pure collagen matrices have been studied for many years [46], and this elongated cell morphology has been amply described in the literature for matrices with similar stiffness [47–51]. It has been further demonstrated that fibroblasts interact with collagen matrices and become entangled with matrix fibrils [52]; previous studies have also shown that the macroscopic matrix deformation results from fibroblast contractile forces that accompany cell elongation [53,54]. When the crosslinking of the alginate backbone reaches a certain threshold (320 Pa), the cells are no longer able to spread inside this biomaterial system, likely because of the increased resistance to deformation of the matrix. Fibroblasts still failed to spread even as the alginate polymeric backbone was further decorated with RGD binding sites in stiffer matrices, suggesting that cell elongation was not limited by the availability of adhesion sites, confirming recent observations of others [55]. Broadly, these results suggest that one can modulate the morphology and contractility of fibroblasts infiltrating a wound dressing simply by controlling the storage modulus of the biomaterial itself. Furthermore, this biomaterial system is likely to be a valuable tool to study the role of mechanical cues in different pathological or developmental contexts in a three-dimensional microenvironment. Two-dimensional substrates have been broadly used to study mechanotransduction mechanisms, but there is increasing evidence that cell morphology, cell–cell and cell–matrix interactions are considerably dependent on culture dimensionality [56,57].

Tuning the storage modulus of the alginate/collagen-I IPN also induced different wound healing-related genetic profiles in dermal fibroblasts, with differential expression of genes related to

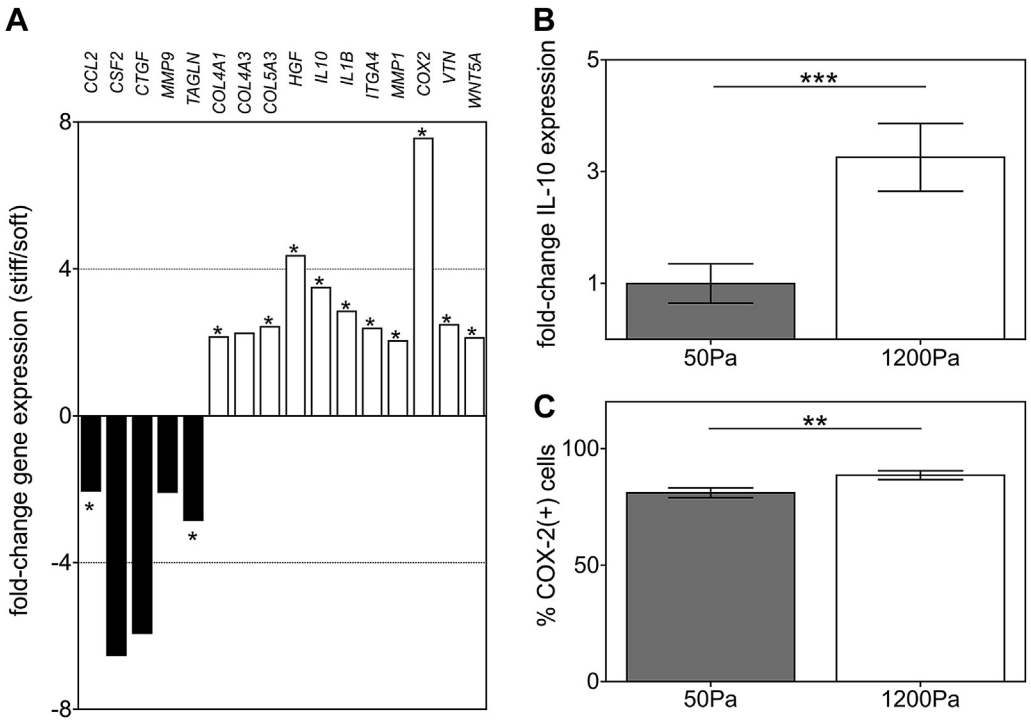

Fig. 6. Different storage moduli promote different wound healing genetic programs, leading to upregulation of inflammation mediators IL-10 and COX-2. (A) Up or downregulation of mRNA expression of fifteen genes involved in the wound healing response by cells encapsulated in IPNs with storage modulus of 50 or 1200 Pa. Data is shown as fold-change in stiff *versus* soft matrices ($n = 3$) (Student's *t* test, $^{*}p < 0.05$). (B) IL-10 production by cells encapsulated in IPNs with storage modulus of 50 or 1200 Pa. Data is shown as fold-change in stiff *versus* soft matrices ($n = 4–6$) (Student's *t* test, $^{***}p < 0.001$). (C) COX-2 antibody staining of cells recovered from IPNs with storage modulus of 50 and 1200 Pa ($n = 3$) (Student's *t* test, $^{*}p < 0.05$). Data are shown as mean and standard deviation. All data was collected after cells were encapsulated for 48 h.

inflammatory cascades, collagen synthesis, surface adhesion receptors and ECM molecules. The downregulation of *CCL2* by fibroblasts encapsulated in stiffer matrices, although not statistically significant, is a noteworthy finding. It has been shown that fibroblasts activate intracellular focal adhesion kinases (FAK) following cutaneous injury, and that FAK acts through extracellular-related kinase (ERK) to trigger the secretion of CCL2 [58]. The failure of fibroblasts to spread in stiffer alginate/collagen-I IPNs is therefore consistent with the downregulated expression of *CCL2*. One of the mechanisms underlying non-healing ulcers is a chronic inflammatory response that is self-sustaining [4]. Therefore the deregulation of key molecular mediators of inflammation is of significant interest for the design of wound dressing biomaterials. The upregulation of COX-2 and IL-10 on stiffer matrices is also a striking finding. COX-2 is known to be responsible for the elevated production of prostanoids in sites of disease and inflammation [59]. IL-10 has a central role in regulating the cytokine network behind inflammation, and is also known to regulate COX-2 during acute inflammatory responses [60]. As inflammation is a key aspect of wound healing [61] the ability of a wound dressing biomaterial to induce or suppress the expression of key orchestrators of inflammation such as IL-10 and COX-2 could be used in the future to guide the outcome of the healing cascade.

The results of this study suggest adjusting the stiffness of a dressing biomaterial placed on a wound site as an approach for skin repair and regeneration. Wound dressing biomaterials deposited at the wound site function simultaneously as a barrier and an external dermal scaffold [62]. We hypothesize that their mechanical properties could potentially be tuned in order to match the required stiffness to aid in repair of the injured skin, even varying by design from site to site, from person to person, or even according to the patient's age. These effects may be even more potent if combined with biomaterial-based, spatiotemporal control over the presentation of bioactive molecules, growth factor or cells [63].

5. Conclusions

An IPN of collagen-I and alginate allows one to control stiffness independently of scaffold architecture, polymer concentration or ligand density. Primary fibroblasts isolated from the dermis of healthy adult patients were able to grow and survive within the interlaced network of these IPNs. Altering the storage modulus led to dramatic changes in the morphology of fibroblasts, and triggered different wound healing genetic programs including altered expression of the inflammation mediators IL-10 and COX-2. Enhancing the number of binding sites to which the fibroblasts can adhere in the IPN does not subdue the effects of mechanics on cell spreading and contraction. These findings suggest that simply tuning the storage modulus of wound dressing biomaterials might allow one to promote or hinder the wound healing response.

Acknowledgments

This work was funded by the BASF Advanced Research Initiative at Harvard University. This work was performed in part at the Center for Nanoscale Systems (CNS), a member of the National Nanotechnology Infrastructure Network (NNIN), which is supported by the National Science Foundation under NSF award no. ECS-0335765. The authors would like to acknowledge Angelo Mao for providing the FITC-labeled alginate, Thomas Ferrante for help with confocal microscopy imaging, the Weitz lab for help/use of rheometer, Anabela Ribeiro Nunes (from the Office for Science Communication at IBMC.INEB) for designing Fig. 1, and Dr. Cathal Kearney for insightful review of this article. C.B.C. had research

fellowships by the Portuguese *Fundação para a Ciência e a Tecnologia* (FCT), Calouste Gulbenkian Foundation (FCG) and Luso-American Development Foundation (FLAD). SK was supported by an HHMI ISRF studentship.

Appendix A. Supplementary data

Supplementary data related to this article can be found at http://dx.doi.org/10.1016/j.biomaterials.2014.06.047.

References

[1] Singer AJ, Clark RAF. Cutaneous wound healing. N Engl J Med 1999;341(10):738–46.
[2] Martin P. Wound healing – aiming for perfect skin regeneration. Science 1997;276(5309):75–81.
[3] Falanga V. Wound healing and its impairment in the diabetic foot. Lancet 2005;366(9498):1736–43.
[4] Menke NB, Ward KR, Witten TM, Bonchev DG, Diegelmann RF. Impaired wound healing. Clin Dermatol 2007;25(1):19–25.
[5] Clark RAF, Ghosh K, Tonnesen MG. Tissue engineering for cutaneous wounds. J Invest Dermatol 2007;127(5):1018–29.
[6] Bell E, Ehrlich HP, Buttle DJ, Nakatsuji T. Living tissue formed in vitro and accepted as skin-equivalent tissue of full thickness. Science 1981;211(4486):1052–4.
[7] Yannas IV, Burke JF, Orgill DP, Skrabut EM. Wound tissue can utilize a polymeric template to synthesize a functional extension of skin. Science 1982;215(4529):174–6.
[8] Yannas IV, Lee E, Orgill DP, Skrabut EM, Murphy GF. Synthesis and characterization of a model extracellular matrix that induces partial regeneration of adult mammalian skin. Proc Natl Acad Sci USA 1989;86(3):933–7.
[9] Zahedi P, Rezaeian I, Ranaei-Siadat S-O, Jafari S-H, Supaphol P. A review on wound dressings with an emphasis on electrospun nanofibrous polymeric bandages. Polym Adv Technol 2010;21(2):77–95.
[10] Boateng JS, Matthews KH, Stevens HNE, Eccleston GM. Wound healing dressings and drug delivery systems: a review. J Pharm Sci 2008;97(8):2892–923.
[11] Wong VW, Akaishi S, Longaker MT, Gurtner GC. Pushing back: wound mechanotransduction in repair and regeneration. J Invest Dermatol 2011;131(11):2186–96.
[12] Wong VW, Paterno J, Sorkin M, Glotzbach JP, Levi K, Januszyk M, et al. Mechanical force prolongs acute inflammation via T-cell-dependent pathways during scar formation. FASEB J 2011;25(12):4498–510.
[14] Wipff P-J, Rifkin DB, Meister J-J, Hinz B. Myofibroblast contraction activates latent TGF-β1 from the extracellular matrix. J Cell Biol 2007;179(6):1311–23.
[15] Zhang H, Landmann F, Zahreddine H, Rodriguez D, Koch M, Labouesse M. A tension-induced mechanotransduction pathway promotes epithelial morphogenesis. Nature 2011;471(7336):99–103.
[16] Boerckel JD, Uhrig BA, Willett NJ, Huebsch N, Guldberg RE. Mechanical regulation of vascular growth and tissue regeneration in vivo. Proc Natl Acad Sci USA 2011;108(37):674–80.
[17] Lo C-M, Wang H-B, Dembo M. Wang Y-l. Cell movement is guided by the rigidity of the substrate. Biophys J 2000;79(1):144–52.
[18] Gardel ML, Sabass B, Ji L, Danuser G, Schwarz US, Waterman CM. Traction stress in focal adhesions correlates biphasically with actin retrograde flow speed. J Cell Biol 2008;183(6):999–1005.
[19] Engler AJ, Sen S, Sweeney HL, Discher DE. Matrix elasticity directs stem cell lineage specification. Cell 2006;126(4):677–89.
[20] Huebsch N, Arany PR, Mao AS, Shvartsman D, Ali OA, Bencherif SA, et al. Harnessing traction-mediated manipulation of the cell/matrix interface to control stem-cell fate. Nat Mater 2010;9(6):518–26.
[21] McNaught AD, Wilkinson AIUPAC. Compendium of chemical terminology. 2nd ed. Oxford: UK Blackwell Scientific Publications; 1997.
[22] Rowley JA, Madlambayan G, Mooney DJ. Alginate hydrogels as synthetic extracellular matrix materials. Biomaterials 1999;20(1):45–53.
[23] Chaudhuri O, Koshy ST, Branco da Cunha C, Shin J-W, Verbeke CS, Allison KH, et al. Extracellular matrix stiffness and composition jointly regulate the induction of malignant phenotypes in mammary epithelium. Nat Mater 2014. http://dx.doi.org/10.1038/nmat4009 [Epub ahead of print], PMID: 24930031.
[24] Chaudhuri O, Parekh SH, Fletcher DA. Reversible stress softening of actin networks. Nature 2007;445(7125):295–8.
[25] Fabry B, Maksym GN, Butler JP, Glogauer M, Navajas D, Fredberg JJ. Scaling the microrheology of living cells. Phys Rev Lett 2001;87(14):148102.
[26] Crank J. The mathematics of diffusion. 2nd ed. Oxford University Press: Clarendon Press; 1979.
[27] Jokinen J, Dadu E, Nykvist P, Käpylä J, White DJ, Ivaska J, et al. Integrin-mediated cell adhesion to type I collagen fibrils. J Biol Chem 2004;279(30):31956–63.
[28] Khetan S, Guvendiren M, Legant WR, Cohen DM, Chen CS, Burdick JA. Degradation-mediated cellular traction directs stem cell fate in covalently crosslinked three-dimensional hydrogels. Nat Mater 2013;12(5):458–65.
[29] Peyton SR, Raub CB, Keschrumrus VP, Putnam AJ. The use of poly(ethylene glycol) hydrogels to investigate the impact of ECM chemistry and mechanics on smooth muscle cells. Biomaterials 2006;27(28):4881–93.
[30] Kloxin AM, Kasko AM, Salinas CN, Anseth KS. Photodegradable hydrogels for dynamic tuning of physical and chemical properties. Science 2009;324(5923):59–63.
[31] Trappmann B, Chen CS. How cells sense extracellular matrix stiffness: a material's perspective. Curr Opin Biotechnol 2013;24(5):948–53.
[32] Park YD, Tirelli N, Hubbell JA. Photopolymerized hyaluronic acid-based hydrogels and interpenetrating networks. Biomaterials 2003;24(6):893–900.
[33] Suri S, Schmidt CE. Photopatterned collagen–hyaluronic acid interpenetrating polymer network hydrogels. Acta Biomater 2009;5(7):2385–97.
[34] Akpalo EBL, Boissière M, Vancaeyzeele C, Fichet O, Larreta- Garde V. Fibrin-polyethylene oxide interpenetrating polymer networks: new selfsupported biomaterials combining the properties of both protein gel and synthetic polymer. Acta Biomater 2011;7(24):2418–27.
[35] Sun J, Xiao W, Tang Y, Li K, Fan H. Biomimetic interpenetrating polymer network hydrogels based on methacrylated alginate and collagen for 3D pre-osteoblast spreading and osteogenic differentiation. Soft Matter 2012;8:2398–404.
[36] Tong X, Yang F. Engineering interpenetrating network hydrogels as biomimetic cell niche with independently tunable biochemical and mechanical properties. Biomaterials 2014;35(6):1807–15.
[37] Ulrich TA, Jain A, Tanner K, MacKay JL, Kumar S. Probing cellular mechanobiology in three-dimensional culture with collagen-agarose matrices. Biomaterials 2010;31(7):1875–84.
[38] Wen C, Lu L, Li X. Mechanically robust gelatin–alginate IPN hydrogels by a combination of enzymatic and ionic crosslinking approaches. Macromol Mater Eng 2013;229(4):504–13.
[39] Edwards C, Marks R. Evaluation of biomechanical properties of human skin. Clin Dermatol 1995;13(4):375–80.
[40] Y-l Yang, Leone LM, Kaufman LJ. Elastic moduli of collagen gels can be predicted from two-dimensional confocal microscopy. Biophys J 2009;97(7):2051–60.
[41] Wu C-C, Ding S-J, Wang Y-H, Tang M-J, Chang H-C. Mechanical properties of collagen gels derived from rats of different ages. J Biomater Sci Polym Ed 2005;16(10):1261–75.
[42] Arevalo RC, Urbach JS, Blair DL. Size-dependent rheology of type-I collagen networks. Biophys J 2010;99(8):L65–7.
[43] Achilli M, Mantovani D. Tailoring mechanical properties of collagen-based scaffolds for vascular tissue engineering: the effects of pH, temperature and ionic strength on gelation. Polymers 2010;2:664–80.
[44] Discher DE, Janmey P. Wang Y-l. Tissue cells feel and respond to the stiffness of their substrate. Science 2005;310(5751):1139–43.
[45] Solon J, Levental I, Sengupta K, Georges PC, Janmey PA. Fibroblast adaptation and stiffness matching to soft elastic substrates. Biophys J 2007;93(12):4453–61.
[46] Elsdale T, Bard J. Collagen substrata for studies on cell behavior. J Cell Biol 1972;54(3):626–37.
[47] Grinnell F. Fibroblast–collagen-matrix contraction: growth-factor signalling and mechanical loading. Trends Cell Biol 2000;10(9):362–5.
[48] Tamariz E, Grinnell F. Modulation of fibroblast morphology and adhesion during collagen matrix remodeling. Mol Biol Cell 2002;13(11):3915–29.
[49] Grinnell F. Fibroblast biology in three-dimensional collagen matrices. Trends Cell Biol 2003;13(5):264–9.
[50] Miron-Mendoza M, Seemann J, Grinnell F. The differential regulation of cell motile activity through matrix stiffness and porosity in three dimensional collagen matrices. Biomaterials 2010;31(25):6425–35.
[51] Dallon JC, Ehrlich HP. A review of fibroblast-populated collagen lattices. Wound Repair Regen 2008;16(4):472–9.
[52] Jiang H, Grinnell F. Cell–matrix entanglement and mechanical anchorage of fibroblasts in three-dimensional collagen matrices. Mol Biol Cell 2005;16(11):5070–6.
[53] Freyman TM, Yannas IV, Pek Y-S, Yokoo R, Gibson LJ. Micromechanics of fibroblast contraction of a collagen-GAG matrix. Exp Cell Res 2001;269(1):140–53.
[54] Eastwood M, Porter R, Khan U, McGrouther G, Brown R. Quantitative analysis of collagen gel contractile forces generated by dermal fibroblasts and the relationship to cell morphology. J Cell Physiol 1996;166(1):33–42.
[55] Maia FR, Fonseca KB, Rodrigues G, Granja PL, Barrias CC. Matrix-driven formation of mesenchymal stem cell-extracellular matrix microtissues on soft alginate hydrogels. Acta Biomater 2014;10(7):3197–208.
[56] Yamada KM, Cukierman E. Modeling tissue morphogenesis and cancer in 3D. Cell 2007;130(4):601–10.
[57] Schwartz MA, Chen CS. Deconstructing dimensionality. Science 2013;339(6118):402–4.
[58] Wong VW, Rustad KC, Akaishi S, Sorkin M, Glotzbach JP, Januszyk M, et al. Focal adhesion kinase links mechanical force to skin fibrosis via inflammatory signaling. Nat Med 2011;18(1):148–52.
[59] Warner TD, Mitchell JA. Cyclooxygenases: new forms, new inhibitors, and lessons from the clinic. FASEB J 2004;18(7):790–804.

[60] Berg DJ, Zhang J, Lauricell DM, Moore SA. IL-10 is a central regulator of cyclooxygenase-2 expression and prostaglandin production. J Immunol 2001;166(4):2674–80.
[61] Eming SA, Krieg Thomas, Davidson Jeffrey M. Inflammation in wound repair: molecular and cellular mechanisms. J Invest Dermatol 2007;127(3):514–25.
[62] MacNeil S. Progress and opportunities for tissue-engineered skin. Nature 2007;445(7130):874–80.
[63] Kearney CJ, Mooney DJ. Macroscale delivery systems for molecular and cellular payloads. Nat Mater 2013;12(11):1004–17.